J Comput Electron (2008) 7: 332–336
DOI 10.1007/s10825-008-0200-z

Three-dimensional simulation of field emission triode structure using carbon-nanotube emitters

Yiming Li · Ta-Ching Yeh

Published online: 28 January 2008

Abstract Field emission (FE) triode arrays with the anodic aluminum oxide (AAO) template carbon nanotubes (CNTs) as the field emitters are successfully fabricated and analyzed. Both the experimental measurement and numerical calculation are conducted to examine the electron conduction properties of AAO-CNTs. Using a three-dimensional finite-difference time-domain particle-in-cell method, a set of Maxwell equations and Lorentz equation is solved self-consistently, where the FE current is computed with Fowler–Nordheim equation. We explore the FE characteristics of AAO-CNTs in the triode structure. After calibration with the measured data, we study the evolution of current density and the convergence of the electron beams on anode plate with different gate voltages, anode heights, and SiO_2 thickness. The current density and focus performance maintain a trade-off relationship, where a larger current density accompanies more divergent electron beam.

Keywords Carbon nanotubes · Anodic aluminum oxide · Field emission · Three-dimensional simulation · Finite-difference time-domain particle-in-cell method · Current density · Electron beam

1 Introduction

Carbon nanotubes (CNTs) are promising for advanced cold-cathode flat panel displays due to their chemical stability, mechanical strength, and electron emission properties [1–3]. A triode type field emission (FE) display possesses more stable and effective emission properties, and higher quality screen, compared with a diode one. To obtain uniform and high FE current, it is necessary to grow vertically aligned CNT arrays on a large area with suitable tube density and diameter. A template method, anodic aluminum oxide (AAO) nano-template, is thus developed [4, 5]. AAO has vertical pore channel, highly ordered pore arrangement, and uniform pore size. FE triode arrays with AAO-CNTs as emitters were fabricated by standard integrated circuit (IC) fabrication process in our recent work [6].

In this article, we employ a three-dimensional (3D) particle-in-cell (PIC) method coupled with the Maxwell equations to simulate the electron emission behavior in the CNT FE triode structure with the AAO template. Effect of the gate voltage, the height of SiO_2(distance between the CNT and the gate), and the anode height in the triode structure are further discussed for the best emission properties.

2 Experiment and simulation

The structure of AAO-CNTs and its cross section on the x–z plane are shown in Fig. 1. To fabricate AAO-CNTs' FE triodes, standard IC processes were used [6]. After the preparation of AAO-CNTs emitters, tetraethoxysilane oxide was deposited on AAO-CNTs' layer as the dielectric layer of the triode by plasma enhanced CVD, and followed by the evaporation-deposition of an Al layer as the gate electrode. The pattern of triodes with a diameter of 6.5 μm was photolithographically defined by a mask aligner. The top layer of Al was etched by a high density plasma reactive ion etch (RIE) system using the gas mixture of BCl3 and Cl2 as the etchant source. The oxide dielectric was then RIE etched using a gas mixture of CHF3 and Ar as the plasma source.

Y. Li (✉) · T.-C. Yeh
Department of Communication Engineering, National Chiao Tung University, Hsinchu, Taiwan
e-mail: ymli@faculty.nctu.edu.tw

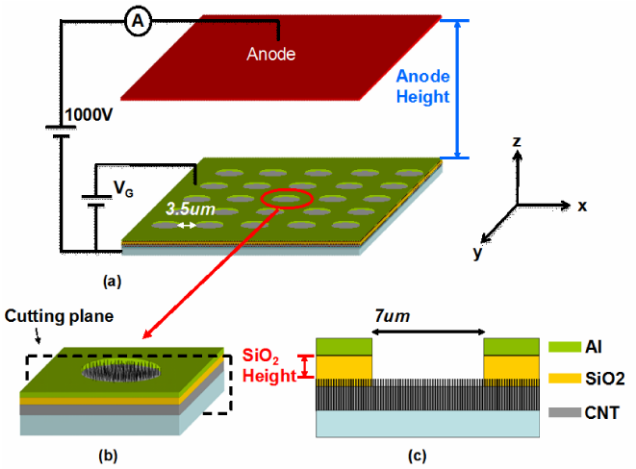

Fig. 1 (**a**) A schematic plot of the structure. (**b**) and (**c**) show a single circle of AAO-CNT and its cross section view

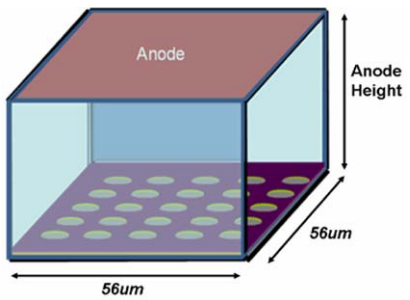

Fig. 2 The entire simulation box includes the whole structure

After the process of RIE, buffered oxide etchant was used to remove the remnant SiO_2. The inset of Fig. 4a shows a SEM image of the fabricated sample. More than 8000 CNTs were grown within a single AAO-CNTs' structure.

To explore the electron-emission properties in AAO-CNTs, the electromagnetic PIC scheme [7, 8] is used. Figure 2 shows the entire simulation box including the whole structure, as shown in Fig. 1a. Starting from a specified initial state, we evaluate the electrostatic field along the emitter surface which is determined for a given geometry and applied voltage. In the FE process, the electron emission is modeled by the Fowler–Nordheim (F–N) equation [9]:

$$J = \frac{A\boldsymbol{E}^2}{\varphi t^2}\exp\left(\frac{-Bv(y)\varphi^{3/2}}{E}\right), \tag{1}$$

where $A = 1.541 \times 10^{-6}$ A eV/V2 and B is a fitting parameter which depends on the applied voltage; $\boldsymbol{E}$ is the normal component of the electric field at the emitter surface, $\varphi = 5$ eV is the work function of the emission material, $t^2 = 1.1$, and $v(y) = 0.95 - y^2$ with $y = 3.79 \times 10^{-5}\boldsymbol{E}^{1/2}/\varphi$ is in SI unit. Determined by (1), the emission current density is function of the local electric field, the work function of emitter material and the fitting parameters. The weighted charge density and current density at the grids are subsequently calculated. The obtained charge density and current density are successively used as sources in the Maxwell equations for advancing the electromagnetic fields. For solving Maxwell equations, we use Yee-cells on a staggered time-grid. We then perform a time integration of the Faraday's law, the Ampere's law, and the non-relativistic Lorentz equation,

$$\begin{cases} \frac{\partial \mathbf{B}}{\partial t} = -\nabla \times \mathbf{E}, \\ \frac{\partial \mathbf{E}}{\partial t} = -\frac{\mathbf{J}}{\varepsilon} + \frac{1}{\mu\varepsilon}\nabla \times \mathbf{B}, \\ \mathbf{F} = q\left(\mathbf{E} + \mathbf{v} \times \mathbf{B}\right), \quad \text{and} \\ \frac{\partial \mathbf{x}}{\partial t} = \mathbf{v}, \end{cases} \tag{2}$$

where the velocity is derived from the deviation of the position of charge particle, subject to constraints provided by Gauss's law and the divergence of $\mathbf{B}$,

$$\nabla \cdot \mathbf{E} = \frac{\rho}{\varepsilon} \quad \text{and} \quad \nabla \cdot \mathbf{B} = 0. \tag{3}$$

We notice that $\mathbf{E}$ and $\mathbf{B}$ are the electric and magnetic fields, $\mathbf{x}$ is the position of charge particle, and $\mathbf{J}$ and ρ are the current density and charge density resulting from charge particles. The time-dependent Maxwell's equations are solved to obtain electromagnetic fields, where the Lorentz equation is solved for non-relativistic particle trajectories. We use a center-difference solution scheme to solve the fully time-dependent Maxwell's equations. It is one of the simplest time-dependent field algorithms. However, center-difference is very susceptible to the high-frequency noise typically produced by relativistic particles. Thus we use the centered-difference algorithm only for non-relativistic particles.

The charge particles are moved according to the Lorentz force $\mathbf{F}$ using the fields advanced in each time step. The procedure is repeated for each time step until the specified number of time steps is reached. The 3D FDTD-PIC, as shown in Fig. 3, thus approaches to self-consistent simulation, where the space-charge effects [10] are automatically included.

3 Results and discussion

Simulated results are calibrated with the measured data before analyzing different structures. Figure 4a shows the measured (solid line) and simulated (dotted line) current-voltage (I–V) curves with the SiO_2 thickness of 0.7 μm, the anode height of 100 μm and the gate voltage (V_G) of 0 V when the anode voltage (V_A) varying from 10 V to 1000 V.

Figure 4b shows the 3D electron trajectories and the cross-sectional plot along the x–z plane. The anode plate collects the current emitted from CNTs. The F–N plot is shown in the inset of Fig. 4a. It indicates the true nature of

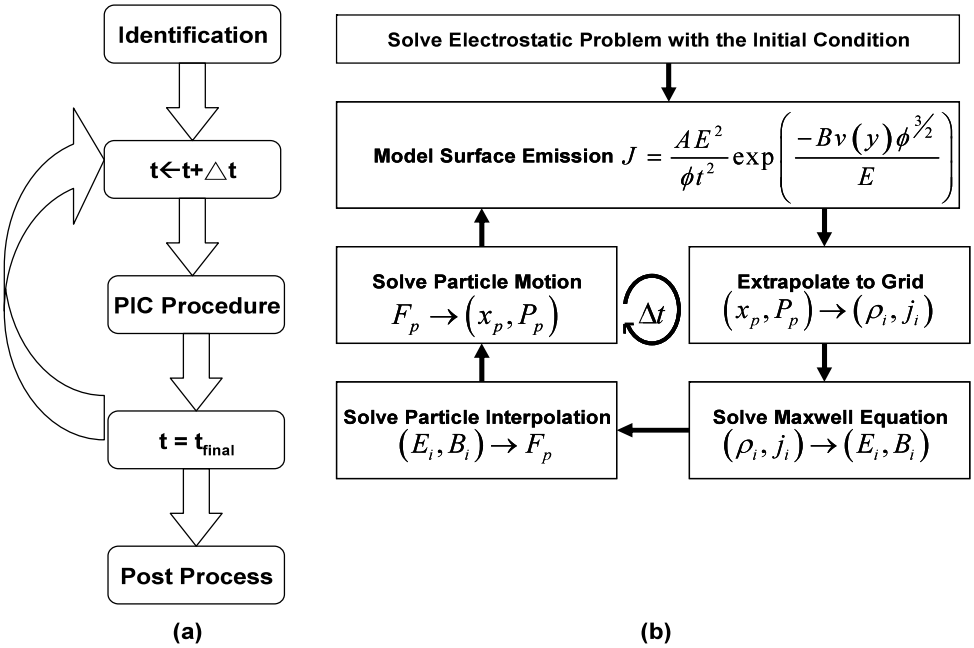

Fig. 3 (**a**) The computational scheme. (**b**) The flowchart of PIC procedure and the corresponding equations

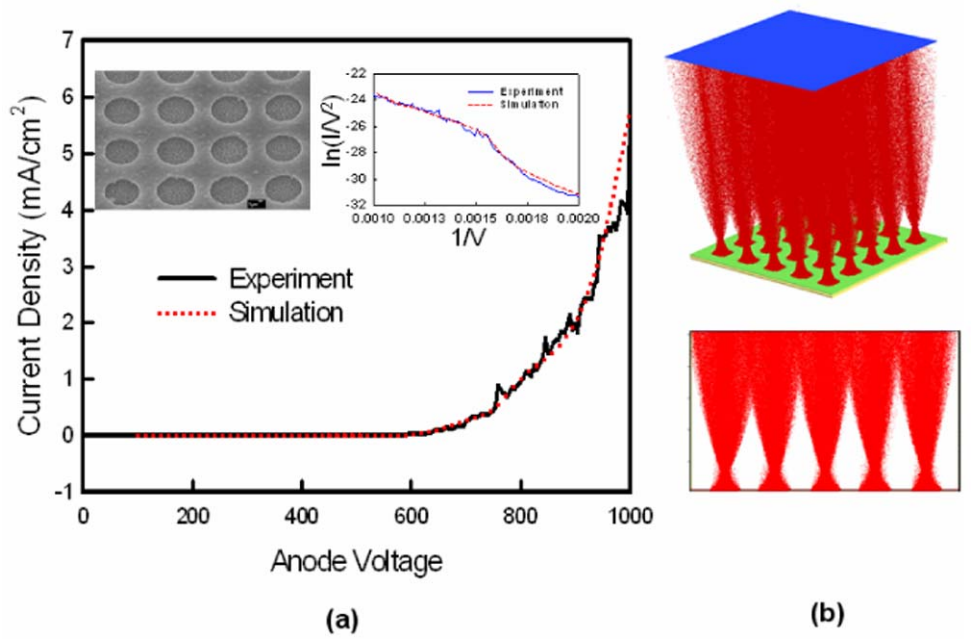

Fig. 4 (**a**) The I–V curve of the CNT device. The SEM image of fabricated AAO-CNT sample and the F–N plot are shown in the *inset*. (**b**) 3D electron trajectories of the AAO-CNTs' structure and the x–z plane with $V_G = 0$ V, $SiO_2 = 0.7$ μm and anode height = 100 μm

FE. The solid line is the experiment data and the dash line is the simulation result using the calibrated model. We are further going to discuss the current density and the convergence of the electron beams on the anode plate with different gate voltages, anode heights, and SiO_2 thickness.

Figure 5a shows the evolution of collected current with different V_G, and Fig. 5b presents the current density versus V_G. The electron beams of the three different gate voltages are shown in the inset. When $V_G = 20$ V, it will have the maximum current and take the least time to get the saturation all over the three. It is because of the higher electric field and larger injection velocity at the anode. But its electron beam divergence seriously and will cause the loss of power. A best focus performance is when $V_G = 9$ V. At this moment, the bundle of the electron beam is close to a cylinder. If we decrease the gate voltage to 2 V, the electron beam will become over-focus and result in divergence on the anode plate.

Figure 6a shows the collected time-dependent current with different anode height. The maximum current is with anode height of 50 μm. It also takes the least time to reach the saturation. The current density as a function of anode

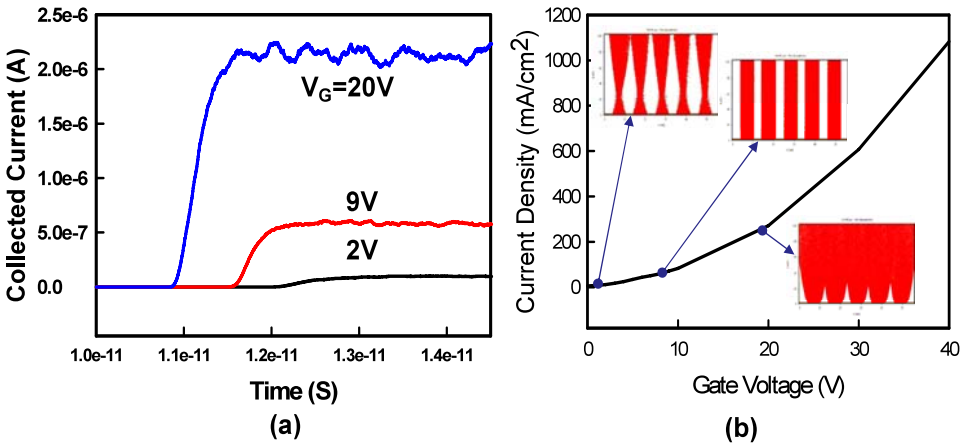

Fig. 5 (**a**) Plot of the collected current with different V_G, where the anode height = 100 μm and the thickness of SiO_2 = 0.7 μm. (**b**) Plot of the saturated current density versus V_G. The electron trajectories of the x–z plane are shown in the *inset*

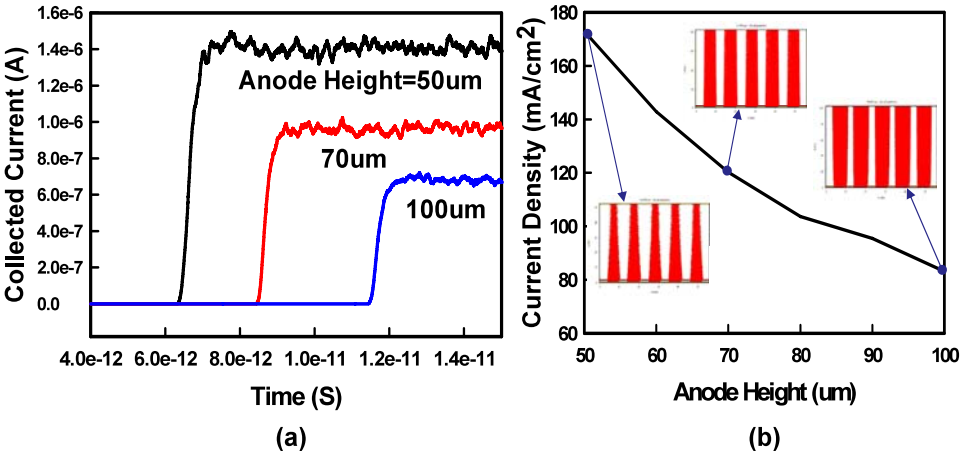

Fig. 6 (**a**) Plot of the collected current with different anode height: 50 μm, 70 μm, 100 μm, where V_G = 10 V and SiO_2 thickness = 0.7 μm. (**b**) Plot of the saturated current density versus the anode height. The electron trajectories of the x–z plane are shown in the *inset*

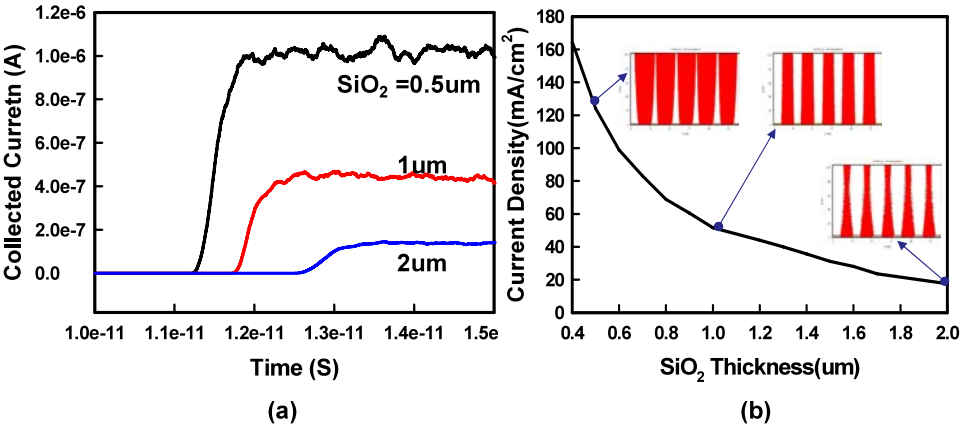

Fig. 7 (**a**) Plot of the collected current with different SiO_2 thickness: 0.5 μm, 1 μm, 2 μm, where anode height = 100 μm and V_G = 10 V. (**b**) Plot of the saturated current density versus SiO_2 thickness. The electron trajectories of the x–z plane are shown in the *inset*

height is shown in Fig. 6b. When the anode height is getting larger, the current density becomes smaller because of the weaker electric field intensity. And it takes longer time to saturate with longer anode height. The focus performance with respect to anode heights, shown in the inset of Fig. 6b, is all under-focus. Nevertheless, when the anode height is 50 μm, it is slightly over-focus, compared with the straight electron beam with the anode height of 70 μm. Figure 7a shows the collected current with different SiO_2 thickness. We find that when the gate is closer to CNT, it will eject more current and faster ejection speed because of the larger electric field intensity. However, Fig. 7b shows that if the gate is very close to CNT, the electron beam will diverge seriously. When the SiO_2 thickness increases to 2 μm, the

Table 1 The current densities and angles of electron beams with different gate voltages, anode heights, and SiO_2 thickness

		Current density (mA/cm^2)	Angle (degree)
Gate voltage (V)	2	12.21	−20
	9	71.49	0
	20	272.14	15
Anode height (μm)	50	172.95	−5
	70	120.2	−1
	100	83.1	3
SiO_2 thickness (μm)	0.5	124.17	5
	1	51.6	0
	2	17.58	−10

Table 2 Affections of current densities from different shapes

	Dimensions (μm^2)	Current density (mA/cm^2)
Circle	38.4835	19.97
Square	38.44	18
Rectangle	38.5	19.58
Trapezoid	38.5	19.64

electron beam will over-focus. An optimal setting on the thickness of SiO_2 is 1 μm. The results are summarized in Table 1.

The shape of a single circle of AAO-CNTs, as shown in the inset of Fig. 4a, may not be a circular form because of the process variation. We have examined the FE property of the structure with different shapes of the cross section of $x-y$ plane, such as circle, square, rectangle, and trapezoid. The environmental settings are the anode height is 100 μm, the gate voltage is 5 V, the anode voltage is 1000 V, and the thickness of SiO_2 is 0.7 μm. As listed in Table 2, we can see when the four shapes have about the same volumes; their current densities are very close. As shown in Fig. 8, we can see that the four shapes are about to have the same collected current and saturation time. So in a certain range the process variation of the shape will not affect the characteristic of the AAO-CNTs much.

4 Conclusions

We have studied the FE property for AAO-CNTs in the triode structure using a FDTD-PIC method. After calibration, we found that the evolution of collected current on the anode as well as the current density depends upon the applied voltage, the thickness of SiO_2, and the distance between the anode and structure. The time for stable collected current is crucial for advanced FE technology. For more specific calculation, we are examining the effect of finite number of CNTs, random height and position of CNTs on FE property.

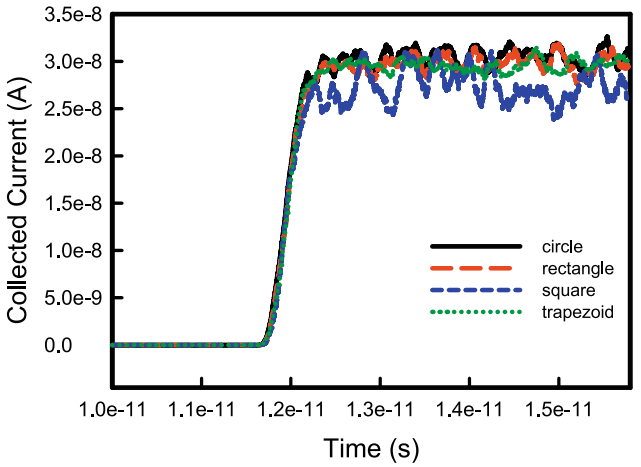

Fig. 8 Collected current and ejection speed versus different shapes of a single circle of AAO-CNTs

Acknowledgements This work was supported in part by Taiwan National Science Council (NSC) under NSC-96-2221-E-009-210 and Contract NSC-96-2752-E-009-003-PAE, and by the ChungHwa Picture Tubes, Ltd., under a 2006–2008 grant. Authors thank Prof. F.-M. Pan for supporting sample characterization.

References

1. Saito, Y., Uemura, S.: Field emission from carbon nanotubes and its application to electron sources. Carbon **38**, 169 (2000)
2. Huh, Y., Lee, J.Y., Lee, J.H., Lee, T.J., Lyu, S.C., Lee, C.J.: Selective growth and field emission of vertically well-aligned carbon nanotubes on hole-patterned silicon substrates. Chem. Phys. Lett. **375**, 388 (2003)
3. Ito, F., Tomihari, Y., Okada, Y., Konuma, K., Okamoto, A.: Carbon-nanotube-based triode-field-emission displays using gated emitter structure. IEEE Electron Device Lett. **22**, 426 (2001)
4. Mei, X., Blumin, M., Kim, D., Wu, Z., Ruda, H.E.: Molecular beam epitaxial growth studies of ordered GaAs nanodot arrays using anodic alumina masks. J. Cryst. Growth **251**, 253 (2003)
5. Chen, P.-L., Kuo, C.-T.: Self-organized titanium oxide nanodot arrays by electrochemical anodization. Appl. Phys. Lett. **82**, 2796 (2003)
6. Lin, C.-C., Chang, K.-C., Pan, F.-M., Kuo, C.-T., Liu, M., Mo, C.-N.: Growth of carbon nanotube field emitters in the triode structure using anodic aluminum oxide as the template. Diam. Relat. Mater. **16**, 1388 (2007)
7. Birdsall, C.K., Langdon, A.B.: Plasma Physics via Computer Simulation. McGraw-Hill, New York (1985)
8. Verboncoeur, J.P., Langdon, A.B., Gladd, N.T.: An object-oriented electromagnetic PIC code. Comput. Phys. Commun. **87**, 199–211 (1995)
9. Fowler, R.H., Nordheim, L.W.: Containing papers of a mathematical and physical character. R. Soc. Proc. A **119**, 173–181 (1928)
10. Stern, T.E., Gossling, B.S., Fowler, R.H.: Further studies in the emission of electrons from cold metals. R. Soc. Proc. A **124**, 699–723 (1929)